Functional laser-induced damage threshold of aluminum coating deposited by magnetron sputtering with different power supply modes Adrien Chauvin*1, Stéphanos Konstantinidis, Jakub Zázvorka, Mojmír Havlík, Lukáš

Adrien Chauvin*¹, Stéphanos Konstantinidis,² Jakub Zázvorka,³ Mojmír Havlík,¹ Lukáš Horák,⁴ Martin Přeček,¹ Ľudovít Haizer,¹ Štěpán Vyhlídka,¹ Milan Dopita,⁴ Martin Veis³ and Daniel Kramer¹

Address: ¹ ELI Beamlines Facility, The Extreme Light Infrastructure ERIC, Za Radnicí 835, 25241 Dolní Břežany, Czech Republic, ² Plasma-Surface Interaction Chemistry, University of Mons, 20 Place du Parc, 7000 Mons, Belgium, ³ Institute of Physics, Faculty of Mathematics and Physics, Charles University, Ke Karlovu 5, Praha, 121 16, Czech Republic, ⁴ and Department of Condensed Matter Physics, Faculty of Mathematics and Physics, Charles University, Ke Karlovu 5, 121 16 Praha 2, Czech Republic.

Email: Adrien Chauvin – adrien.chauvin@eli-beams.eu

^{*} Corresponding author

This is the author's peer reviewed, accepted manuscript. However, the online version of record will be diffe PLEASE CITE THIS ARTICLE AS DOI: 10.1063/5.0295260

Abstract

The need for high-power, high-intensity laser facilities has driven the scientific community to develop optics capable of withstanding higher fluences. The main challenge in increasing power levels is the limited damage threshold of optics. In this paper, we report the laserinduced damage threshold (LIDT) of aluminum coatings deposited via magnetron sputtering. Aluminum coatings (150 nm) were investigated as 45° s-polarization mirrors, a geometry widely employed for beam steering in high-power laser systems. The coatings were produced using three plasma techniques: direct-current (DCMS), radiofrequency (RFMS), and highpower impulse (HiPIMS). Our results show that the RFMS coating is rougher than the DCMS and HiPIMS coatings, which affects its reflectance efficiency (at 45° in s-polarization), even at 1060 nm, decreasing from 96% for DCMS and HiPIMS to 91% for RFMS. 1k-on-1 LIDT tests using a femtosecond laser beam (110 fs) at 1060 nm demonstrate that coatings deposited by HiPIMS and DCMS withstand higher fluences (0.260 J/cm²) compared to RFMS (0.112 J/cm²). Finally, the LIDT performance was compared with the Functional LIDT (F-LIDT), defined as the incident fluence at which the reflected beam decreases by less than 5%. In this study, we observed a discrepancy between the 1k-on-1 LIDT and the F-LIDT values for DCMS and HiPIMS. The F-LIDT for DCMS was higher (0.288 J/cm²) than that of HiPIMS (0.232 J/cm²), which may be partly attributed to the larger crystallite size observed in DCMS. Additionally, the potential use of the HiPIMS power supply mode for developing highperformance optical coatings is discussed.

Keywords

LIDT, HiPIMS, sputtering, aluminum, F-LIDT

manuscript. However, the online version of record will be different from this version once it has been copyedited and typeset. PLEASE CITE THIS ARTICLE AS DOI: 10.1063/5.0295260

This is the author's peer reviewed, accepted manuscript. However,

1 Introduction

The race towards higher laser damage thresholds for optics for high-power lasers has led to a better understanding of the laser-induced damage (LID) process in coatings. LID corresponds to the permanent change in the material structure resulting from a significant displacement of atoms. There are several physical processes involved when a laser beam hits the surface of a material, from the laser absorption to the atomic motion that induces LID. In the case of a metal film, when irradiated by the laser, the free electrons strongly absorb the laser energy. The energy dissipation is done by electron de-excitation via electron-electron collisions, followed by electron-phonon collisions to release the energy into the surrounding lattice and reach thermal equilibrium. During the energy dissipation stage, stress and distortion of the material occur up to catastrophic damage due to mechanical failure, melting of the surface, or a combination of both.²⁻⁴ This model is valid for the rather long pulse regime (i.e., nanosecond and longer). However, in the femtosecond pulses regime, the time scale of the energy dissipation is lower or comparable to the one of the pulses, thus the electrons do not have enough time to transfer their energy to the lattice.⁵ In this case, the LID appears due to the fast ionization of atoms (via multi-photon ionization) and the acceleration of the free electrons, which leads to the ejection of materials by Coulomb explosion.^{2,6}

Considering this understanding, a few key parameters need to be taken into account for the design of coatings that can withstand high laser energy with various pulse durations without showing LID. First, the LID occurs due to the absorption of energy from the laser by the coating. To minimize this absorption, one can reduce the roughness of the coating. A rough surface increases diffuse scattering and promotes multiple internal reflections, which enhances the optical path length within the material and thereby increases absorption. On the other side, for a flat surface, more light undergoes specular reflection and less is absorbed.^{7,8} Second, the presence of localized defects (i.e., cracks, grooves, pores, inclusions) is a major

source of LID in optical coatings. ^{9,10} In metallic coating, the defects localized near the surface are the most critical. ¹ The absorption of the laser energy by a defect may induce two main processes: i) the build-up of a local thermal and mechanical stress, and ii) the amplification of the electric field in the vicinity of the defect, leading to the melting or the fracturing of the coating. ¹ Third, excessive residual stress in the coatings causes the film to crack and ultimately leads to the LID. These stresses result from many sources, including differences in coefficients of thermal expansion of the substrate and film materials, intrinsic stresses related to the film deposition process, and other contributions related to the growth and the interface between the substrate and the thin film. ¹¹ Finally, mostly for longer laser pulse durations, the localized temperature rise due to the dissipation of energy leads to LID. According to the one-dimensional heat flow calculation estimation, this effect can be mitigated by increasing the density of the coating. ¹ Overall, an effective metallic coating should have low absorption, a low number of defects, low residual stress, and be rather dense.

To design such optical coatings, many deposition approaches are available nowadays. For example, the reports from the damage competitions¹² highlight eight different thin film deposition techniques, which can be categorized into three groups, namely: thermal evaporation, sputtering, and solution deposition. Each technique shows pros and cons when it comes to a dedicated application.¹² If we focus on conventional magnetron sputtering (MS) processes - Direct-Current (DC), or Radiofrequency (RF) -, the relatively low quality of the coatings limits the LIDT. To overcome this drawback, one can bombard the coating with neutral atoms or ions during the growth to increase the density and decrease the defect generation.^{13,14} Due to the relatively low degree of ionization of sputtered species (less than 1%) in conventional MS, most of the charged bombarding particles are made of Ar⁺ ions.¹⁵ However, the bombardment of the film by Ar⁺ can be detrimental since it can cause the subplantation of the Ar atoms in the film.¹⁶ This subplantation can lead to the formation of lattice defects, high residual stresses, and a deterioration of the quality of the film/substrate

interface. ^{14,17} The deployment of high-power pulsed plasma sources (i.e., high-power impulse - HiPIMS) allows for a considerably higher total ion flux composed of metallic ions to the substrate and a sputtered material ionization of up to 80%. ^{14,18} Therefore, HiPIMS allows the creation of a denser coating with lower roughness compared to conventional magnetron sputtering (DC or RF). ^{19,20} Moreover, HiPIMS coatings show a lower residual stress after deposition compared to Ion-beam-assisted deposition techniques (IBAD). ²¹

A key issue for efficient coating design of optical components involved in laser-material interaction applications is the accurate determination of the laser-induced damage threshold (LIDT). LIDT is defined as the minimum laser peak fluence for which an observable modification occurs. In principle, this minimal surface damage is related to LID. Various standard and accurate methods for the estimation of the LIDT have been developed.^{22,23} One of the most important detection techniques recommended in the ISO 21254 is the incident light microscope with the Nomarski-type differential interference contrast (DIC).²⁴ However, it has been pointed out that only analysis by DIC microscope is not enough since it assumes that the usability of the coating is lost when any changes can be seen. Thus, discussions have been made in the community to integrate the functional LIDT (F-LIDT), which takes into account the evolution of the properties of the coating during the test.²⁵

In this paper, we report the LIDT and F-LIDT of optical coatings deposited using magnetron sputtering processes, using three different plasma generation modes: DC, RF, and HiPIMS. The coatings were tested at 45° in s-polarization. Mirrors operating at this geometry are widely used in high-power laser facilities for beam transport and diagnostics, ²⁶ and must therefore withstand high fluence without compromising reflectivity. Aluminum is particularly attractive for such applications due to its broad reflectance from the UV to NIR, minimal group-delay dispersion (GDD), relatively low cost compared to noble-metal coatings, and reduced environmental impact.²⁷ Unlike multilayer dielectric (MLD) mirrors, which are

This is the author's peer reviewed, accepted manuscript. However, the online version of record will be diffe PLEASE CITE THIS ARTICLE AS DOI: 10.1063/5.0295260 optimized for narrow spectral ranges and specific incidence conditions,²⁸ metallic coatings provide broadband and versatile performance, making Al particularly attractive for steering mirrors in ultrafast laser systems.²⁹ We compare the morphology, residual stress, and optical properties of an aluminum thin film grown on fused silica by these three approaches using the same parameters (i.e., average power, deposition pressure, and targeted thickness). A femtosecond laser (110 fs) operating at 1060 nm has been used to compare the LIDT for each coating. Moreover, the reflected beam has been probed during LIDT to get the evolution of the F-LIDT.

2 Experimental

2.1 Deposition of the aluminum coating

Aluminum thin films (~ 150 nm) were deposited using three different magnetron sputtering processes on a 2.54 cm diameter fused silica substrate (Optoman, Lithuania). The substrates were cleaned in an ultrasonic bath with a 5% DeContam® (EPSI Metals, USA) solution, followed by rinsing in demineralized water before each deposition. Depositions took place in a vacuum chamber with a base pressure of 10⁻⁸ mbar, equipped with an aluminum target (99,99 % purity) with a diameter of 5.08 cm mounted on a magnetron positioned 20.7 cm from the substrate. The magnetron was operated with a MAGPULS MP2-20 (Magpuls, Germany) power supply, enabling deposition in either DC or HiPIMS modes. For RF sputtering, a COMET Cito Plus (Comet AG, Switzerland) generator was used. The deposition rate and film thickness were determined in-situ during deposition using a quartz crystal microbalance (QCM) sensor integrated in the chamber. The QCM measures the change in resonance frequency of a quartz crystal as material accumulates on its surface, which can be directly converted into deposited thickness using the known density of the film material.³⁰ This technique is widely used for sputtered films and provides reliable real-time monitoring of

the deposition process.³¹ The substrate remained at floating potential and was maintained at a constant temperature of 23°C. The deposition pressure was fixed at 0.5 Pa, with an argon flow of 20 sccm and substrate rotation at 10 rpm. The average power applied to the target was 35 W across all three techniques. For DCMS, the target voltage was 325 V with a current of 0.1 A, resulting in a deposition rate of 0.72 nm/min. RFMS operated at 157 V with a deposition rate of 0.36 nm/min. For HiPIMS, a unipolar pulse of -575 V with a 50 µs pulse duration and a 1% duty cycle was applied to the cathode. The peak current reached 15 A, corresponding to a peak target current density of approximately 0.72 A/cm², with a resulting deposition rate of 0.6 nm/min.

2.2 Characterization

Scanning electron microscopy (SEM) was performed in a Thermo Scientific - FEI Quattro S with an acceleration voltage of 5 kV.

Surface roughness was measured using a Zygo interferometer DynaFiz® operating at 633 nm in DynaPhase mode. Tilt and piston were removed using Zernike polynomial subtraction. A high-pass kernel convolution filter (median type, size 49) was applied to isolate the roughness component. The roughness was quantified over a circular area of 20 mm in diameter, and the reported values correspond to root mean square roughness (R_q).

The X-ray diffraction (XRD) measurements were conducted both in a parallel beam and Bragg-Brentano setup using a Rigaku SmartLab diffractometer equipped with a 9 kW rotating anode Cu source generating K α radiation (wavelength $\lambda = 0.15418$ nm). It included a set of 5° Soller slits to eliminate axial divergence in both the primary and diffracted beams, and a 2D hybrid pixel single-photon counting HyPix3000 detector. The XRD patterns were measured over a 2 θ range from 20° to 120° with a step size of 0.01°. Two fixed incident angles of 1° and 0.23° were used for the measurement in parallel beam setup. The parasitic wavelengths W

PLEASE CITE THIS ARTICLE AS DOI: 10.1063/5.0295260

is the author's peer reviewed, accepted manuscript. However,

L α and Cu K β K from the X-ray tube produce weak twins of the peaks at lower 2 θ , those were identified and ignored for the Rietveld analysis.

The optical properties were measured with a spectrophotometer Photon RT by Essent Optics, with an angle of 45°, from 250 to 1500 nm, and with s-polarized light.

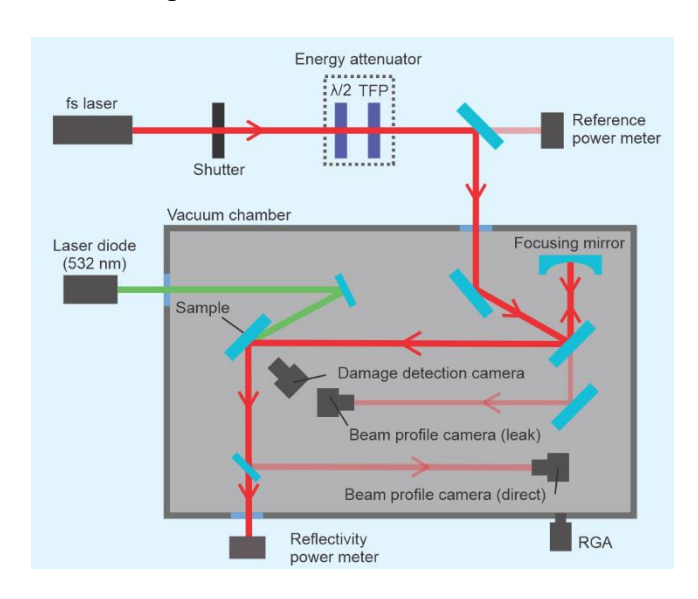


Figure 1: Schematic of the LIDT setup used in this study. $\lambda/2$: half-wave plate, TFP: Thin Film Polarizer, RGA: Residual Gas Analysis.

The laser damage threshold (LIDT) experiments were performed using the L4 ATON frontend at ELI-Beamlines operating at a wavelength of 1060 nm, a repetition rate of 5 Hz, and a pulse duration of 110 +/- 10 fs. The characteristics of the beam (Figure S1) have been recorded with a Few Cycles Spectral Phase Interferometry for Direct Electric-field Reconstruction (FC SPIDER, APE, Germany), which provides both spectrum and temporal pulse characterization. The three 1-inch samples were mounted on a two-dimensional translational stage and a rotational stage. The LIDT experiments were carried out at an angle of incidence (AOI) of 45 degrees between the normal of the substrate and the incoming beam. The laser beam was focused on the sample surface using spherical focusing mirror (focal length of 80 cm) to a beam diameter of 165 μm. The setup details are displayed in Figure 1.

light captured by the detection camera. The polarizer was a broadband thin-film polarizer placed at 70° incidence. The LIDT experiments were performed in a vacuum chamber evacuated using a primary pump and a turbomolecular pump, reaching ~10⁻⁶ mbar. Further details of the setup can be found in our previous work.³² A quadrupole mass spectrometer was used to monitor the residual gas (RGA) during the experiments. The typical RGA spectrum before the LIDT experiment is provided in Figure S2. The LIDT of the coatings was evaluated following ISO 21254 standard procedures.³³ Two complementary protocols were applied: (i) R-on-1 (ramp test): the same site is irradiated while progressively ramping the laser fluence until the first permanent damage is observed. This method is sensitive to laser conditioning effects, where progressive exposure to sub-threshold fluences can slightly modify the coating prior to failure. (ii) S-on-1 (multishot test): a site is exposed to a fixed number of pulses at constant fluence, and a new site is then tested at a higher fluence. In this study, each site was exposed to 1000 consecutive pulses (1k-on-1), which is particularly relevant for functional LIDT (F-LIDT) assessment, as it probes long-term resistance and cumulative damage mechanisms. The combination of these methods provides complementary insight: R-on-1 captures conditioning behavior, while 1k-on-1 evaluates resistance under extended irradiation. We monitored the laser damage online through continuous laser scattering from the irradiated spot, in which changes triggered the beam to abort. The damage morphologies were characterized ex-situ by an Olympus OLS5100 microscope in differential interference contrast (DIC) configuration. The LIDT measurements were performed at three positions on each sample. The reported uncertainties include the fitting error, estimated as half the transition width (difference between the lowest damaged and highest undamaged fluence), and independent contributions from pulse-to-pulse energy fluctuations (\approx 1%), spatial variations ($\approx 2\%$), and system calibration ($\approx 5\%$). All contributions were combined using rootsum-square (RSS) to yield the total standard uncertainty.

PLEASE CITE THIS ARTICLE AS DOI: 10.1063/5.0295260

This is the author's peer reviewed, accepted manuscript. However,

3 Results and Discussion

3.1 Characterization of Aluminum thin films

3.1.1 Microstructure of the thin films. First, the thickness of the film has been fixed ~ 150 nm since the expected loss of energy by transmittance for aluminum is negligible (lower than 10^{-8}) for this thickness.³⁴ Moreover, the theoretical calculation showed that the damage threshold reaches a plateau for thicknesses over 150 nm in thickness.⁴ To deposit the films, the deposition rate has been measured for each discharge mode. The fastest deposition rate is observed for DCMS (i.e., 0.72 nm.min^{-1}), followed by HiPIMS (i.e., 0.6 nm.min^{-1}) and finally RFMS (i.e., 0.36 nm.min^{-1}). Samuelson et al.³⁵ reported a deposition rate ratio between DCMS and HiPIMS for aluminum around ~ 0.83 , and according to Nyaiesh et al.,³⁶ the deposition rate ratio between DCMS and RFMS is ~ 0.5 . However, in our case, the observed drop in deposition rate for RFMS may also result from power dissipation in the impedance matching box, despite the controller reporting a low reflected power at the target (2 W). The decrease in deposition rate between DCMS and HiPIMS samples would highlight the effective ionization of the target.

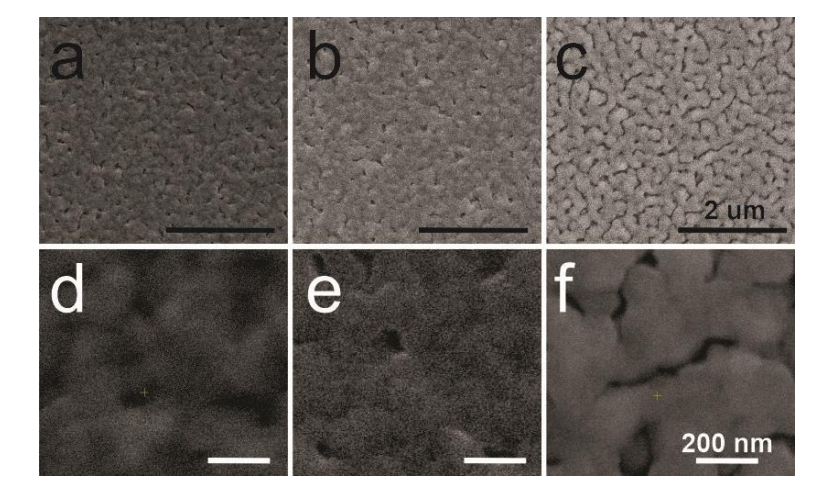


Figure 2: SEM micrographs at (a-c) low and (d-f) high magnification of the surface of the aluminum deposited on fused silica by (a, d) DCMS, (b, e) HiPIMS, and (c, f) RFMS.

the online version of record will be different from this version once it has been copyedited and typeset. This is the author's peer reviewed, accepted manuscript. However, the online version of record will be diffe PLEASE CITE THIS ARTICLE AS DOI: 10.1063/5.0295260

The film topography observed by SEM is very similar to aluminum coatings made by electron beam evaporation.³⁷ The aluminum coatings made by DCMS and HiPIMS reveal a collection of close-packed, apparently rounded protusions. The aluminum sample made by RFMS shows a more open structure, suggesting an increase in the roughness. The roughness of the samples has been evaluated by interferometric measurements. As expected, the aluminum sample deposited by RFMS is rougher than DCMS and HiPIMS, with an RMS value of 29, 4, and 2 nm, respectively (Figure S3, Table 1). This difference in morphology may result from changes in adatom energy and/or enhanced bombardment by energetic particles, including backscattered fast neutrals originating from Ar⁺ ions accelerated in the cathode sheath. In DCMS, the Ar⁺ ions, accelerated to the target, have more energy due to the steady electric field compared to RFMS. Although the Ion Energy Distribution Function (IEDF) in RFMS is shifted to higher energy, resulting in a higher plasma potential, the kinetic energy of the sputtered adatoms is higher in DCMS due to the consistent acceleration provided by the steady electric field. When the adatoms arrive at the substrate, they will diffuse according to their energy. For DCMS, the higher adatom energy and momentum transfer from energetic particles to film atoms contribute to the formation of a denser film, whereas RFMS tends to produce a rougher surface morphology. The similarity in morphology between the DCMS and HiPIMS coating is also due to the high energy of the sputtered adatoms and bombarding particles. In the case of HiPIMS, a denser and less rough coating is expected. However, in this study, for the HiPIMS deposition, the current density was limited to 0.72 A/cm² and the peak power density to 0.4 kW/cm², which is rather low to ensure a sufficient ionization of the target material. 13,14

PLEASE CITE THIS ARTICLE AS DOI: 10.1063/5.0295260

This is the author's peer reviewed, accepted manuscript. However,

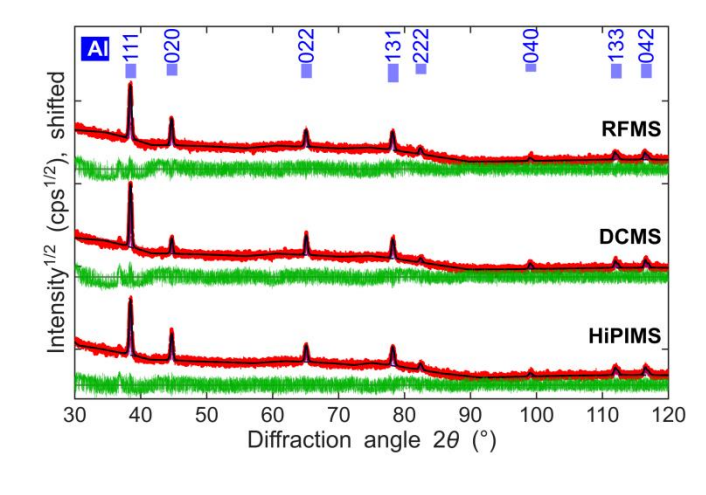


Figure 3: XRD pattern of the aluminum coating deposited by (top) RFMS, (middle) DCMS, and (bottom) HiPIMS. Data collected in a parallel beam setup at a fixed incidence angle of 1°. (red) Experimental data are fitted by (black) Rietveld fit and their (green) difference. The diffractograms are plotted with identical y-axis scaling; curves are offset vertically for clarity.

To probe the film phase constitution, XRD analysis has been carried out on each coating (Figure 3). The lattice parameter, obtained through Rietveld refinement of the XRD patterns, ³⁸ is consistent with that of pure aluminum (4.0504 Å) for both DCMS and HiPIMS, whereas RFMS exhibits a slightly larger value (4.0522 Å, see Table 1). The angular dependence of the peak broadening corresponds to the absence of the microstrain in all samples. The crystallite size remains nearly constant for HiPIMS and RFMS, at approximately 50 ± 2 nm, while DCMS results in significantly larger crystallites, around 80 ± 5 nm. Similar trends have been reported in the literature, where HiPIMS leads to smaller grains compared to DCMS in the sputtering of materials such as copper and tungsten. ³⁹ A comparable behavior has also been observed between RFMS and DCMS in the deposition of molybdenum films. ⁴⁰

The physical origins of these observations differ: in HiPIMS, the energetic ion bombardment interferes with crystal growth, thereby inhibiting the development of larger grains.^{39,41} In RFMS, the reduced deposition rate compared to DCMS yields to smaller crystallites.⁴⁰ In contrast, DCMS, with weaker ion bombardment and a higher deposition rates, allows more

This is the author's peer reviewed, accepted manuscript. However, the online version of record will be diffe PLEASE CITE THIS ARTICLE AS DOI: 10.1063/5.0295260

extensive coalescence and produces larger grains. These results highlight that crystallite size is not governed by deposition rate alone, but by the interplay of deposition kinetics and ion bombardment during growth. Residual stress, as determined by Rietveld refinement, reveals low compressive values for both RFMS and HiPIMS, whereas the DCMS film remains nearly stress-free. In aluminum coatings, it has been reported that residual stress evolves from tensile to compressive with

increasing thickness and can partially relax during interruptions in film growth.⁴² In our case, the compressive stress in HiPIMS films can be linked to atomic peening induced by ion bombardment,^{43,44} while in RFMS the low deposition rate favors densification and the compressive stress. By contrast, the weaker bombardment and high deposition rate in DCMS

permits partial relaxation, resulting in a nearly stress-free state.

It is important to emphasize that the absolute values of residual stress are low (few tens of MPa), and the differences between the three samples are not significant. For DCMS, the stress is very close to zero, which explains the large relative error observed in this case: small absolute fluctuations in the measurement translate into a high uncertainty percentage. Therefore, no unambiguous correlation between residual stress and LIDT can be drawn. These differences in crystallite size and stress are consistent with the observed surface morphology: higher deposition rates in DCMS promote smoother surfaces with larger grains, while lower deposition rates in RFMS lead to smaller grains and increased roughness. HiPIMS, with energetic ion bombardment, modifies surface morphology through densification and occasional subsurface features.

Name	Lattice	Crystallite	Residual	Roughness	Reflectance	LIDT R-	LIDT 1k-	F-LIDT
	parameter	size (nm)	stress (MPa)	RMS (nm)	at 1060 nm	on-1	on-1	(J/cm ²)
	(Å)				S-pol (%)	(J/cm ²)	(J/cm ²)	
DCMS	4.0504 (±	80 (± 5)	-4 (± 10)	4	96.3	0.551 (+/-	0.260 (+/-	0.288 (+/-
	0.0006)					0.046)	0.015)	0.016)

PLEASE CITE THIS ARTICLE AS DOI: 10.1063/5.0295260

This is the author's peer reviewed, accepted manuscript. However,

RFMS	4.0522 (±	48 (± 2)	-22 (± 6)	29	91.0	0.632 (+/-	0.112 (+/-	< 0.112
	0.0006)					0.150)	0.011)	(+/- 0.011)
HiPIMS	4.0508 (±	48 (± 2)	-18 (± 6)	2	95.9	0.584 (+/-	0.262 (+/-	0.232 (+/-
	0.0006)					0.042)	0.015)	0.013)

Table 1: Summary of the characteristics of the aluminum coating deposited on fused silica. F-LIDT corresponds to the highest fluence below which the fluence, after 1000 shots, of the reflected beam is higher than 95% compared to the fluence of the first shot.

3.1.2 Optical properties of thin films. Reflection measurements with s-polarized light and with an incident angle of 45° were carried out to probe the optical properties of the coating, since the latter are aimed at a mirror (Figure 4).

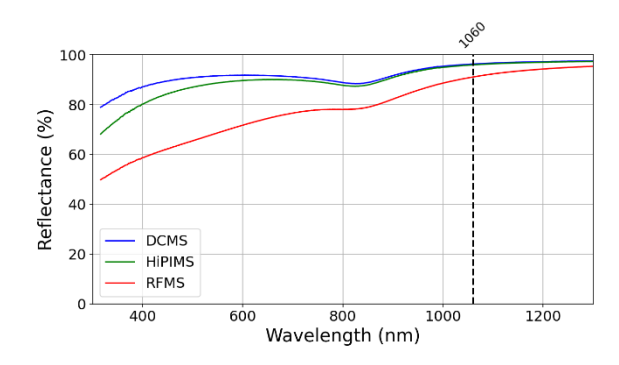


Figure 4: Specular reflectance spectra for s-polarized light with an incident angle of 45°

The behavior of the specular reflectance for the three samples is typical for aluminum coatings, i.e., with a dip corresponding to an absorption peak at around 800 nm due to interband transitions. The low reflectance of the RFMS sample is due to the roughness of the sample (Figure 2). The roughness increases the diffuse reflection and consequently decreases the specular one. For DCMS and HiPIMS samples, the lower the wavelength, the higher the difference in reflectivity. For shorter wavelengths, the DCMS sample has a higher specular reflectivity. This difference suggests that, despite similar roughness, the HiPIMS sample may have more surface or subsurface features, 45 contributing to increased diffuse scattering, leading to reduced specular reflectivity. For the wavelength of LIDT analysis (i.e., 1060)

nm), the reflectance is similar for DCMS and HiPIMS at 96.3% and 95.9% respectively, similar to the one reported in the literature.⁴⁸

3.2 Laser-induced damage threshold (LIDT)

3.2.1 Damage analysis. After the characterization of each coating, the LIDT experiment was carried out on each sample to determine the highest fluence that it can withstand. The damage mechanism in the femtosecond regime, used in this study, is a non-thermal process. For aluminum, the electron-phonon relaxation is around 1 ps, which means that during the laser pulse, the energy is first transferred to the electrons without significant heating of the lattice. This energy transfer creates hot electrons, which further absorb energy and lead to ultrafast ionization. When the density of these laser-generated free electrons reaches the critical plasma density, a dense plasma forms. ^{49–51} This plasma expands and causes material ejection by the Coulomb explosion. To probe the LIDT, two types of tests have been done, namely R-on-1 and S-on-1. The R-on-1 analysis allows for the evaluation of the maximum fluence that the coating can handle while enabling conditioning effects. The S-on-1 reports the durability of the coating after repeated shots.

PLEASE CITE THIS ARTICLE AS DOI: 10.1063/5.0295260

This is the author's peer reviewed, accepted manuscript. However,

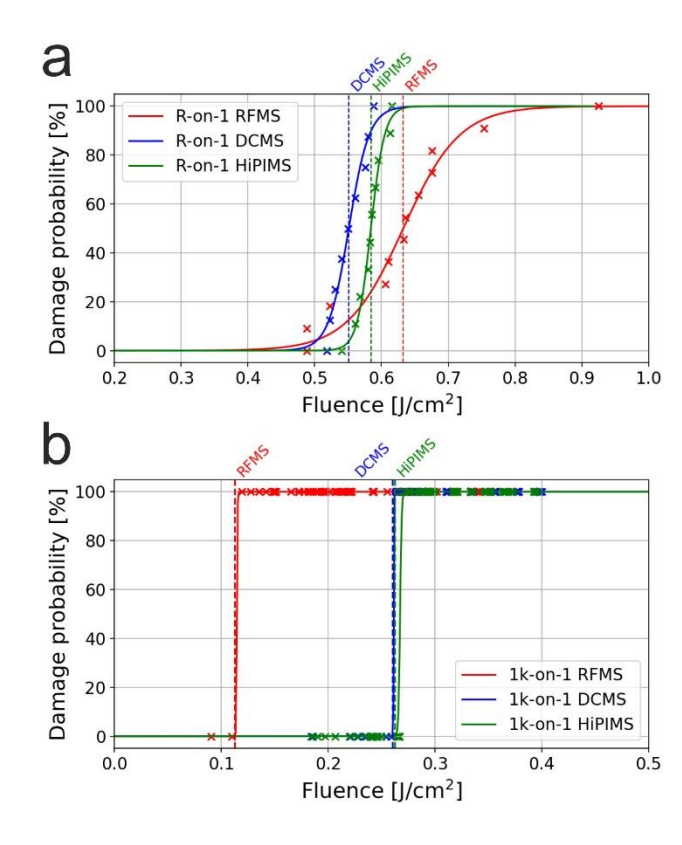


Figure 5: (a) R-on-1 test and (b) 1k-on-1 test. Catastrophic damage probability of the aluminum coating deposited by (blue) DCMS, (red) RFMS, and (green) HiPIMS

Figure 5a reports the R-on-1 analysis of the coating. The LIDT in R-on-1 of the RFMS deposited aluminum film is the highest at 0.632 J/cm²; however, the damage probability spans over a large range with an uncertainty of +/- 0.150 J/cm². The R-on-1 LIDT of the RFMS and HiPIMS deposited aluminum coating are very similar, around 0.550 J/cm². Then the S-on-1 experiments were carried out on each coating. The number of maximum shots was fixed to 1000 (1k-on-1). Figure 5b (and Figure S5) shows the damage probability according to the fluence for each coating. Besides a higher LIDT in the R-on-1 procedure, the 1k-on-1 LIDT of the RFMS deposited aluminum film is the lowest at 0.112 J/cm². This low LIDT value is linked to the high roughness, which is detrimental for fs-laser coating applications. Indeed, for smoother coating, i.e., DCMS and HiPIMS, the value of LIDT is higher at around 0.260 J/cm². This behavior is also correlated with the optical properties of the coatings since the DCMS and HiPIMS coatings have a higher reflectance than RFMS, i.e., 96% and 91%

respectively (Figure 4). The rough coating absorbs more radiation from the laser and thus triggers the damage at a lower fluence than the smooth counterpart. This observation is also supported by the similar LIDT between HiPIMS and DCMS deposited aluminum coating. Overall, the values for the LIDT are in the range of those anticipated by theoretical studies, which evaluate the LIDT around 0.25 J/cm² for a 150 nm thick aluminum coating irradiated by a 1026 nm, 170 fs laser beam.⁴ The discrepancy between the R-on-1 LIDT and 1k-on-1 LIDT for the RFMS deposited aluminum might be due to the low reflectance of the sample. The R-on-1 LIDT is determined when the damage is detected using the scattered light of a laser diode (532 nm - Figure 1), compared to the 1k-on-1, where the evaluation is made afterwards (ex-situ). However, this coating is absorbing in the visible range. Thus, the scattered light might be harder to catch by the camera, resulting in delaying the damage detection for the R-on-1 procedure.

3.2.2 Reflectance properties. The LIDT values reported above are not sufficient to evaluate the efficiency of a coating, since the main aim of a mirror is to reflect the light effectively. A discrepancy between the damage threshold reported by the standard ISO procedure and the functional threshold (F-LIDT), i.e., a decrease in the performance of the coating, can arise. To probe the F-LIDT, the fluence of the reflected beam has been recorded during the 1k-on-1 procedure (Figure 6).

This is the author's peer reviewed, accepted manuscript. However, the online version of record will be different from this version once it has been copyedited and typeset. a Energy ratio 0.7 0.6 400 600 Number of pulses 800 1000 b Energy ratio PLEASE CITE THIS ARTICLE AS DOI: 10.1063/5.0295260 0.7 400 600 Number of pulses 200 C Energy ratio 0.7 0.6 Number of pulses d 0.325 0.300 0.275 0.250 0.225 0.200 0.200 0.27 HiPIMS DCMS RFMS RFMS 0.80 0.85 0.90 0.95 Energy ratio after 1000 shots 0.70 1.00

Figure 6: (a-c) In-situ measurement of the reflected energy normalized to the first reflected pulse during the 1k-on-1 test showing the decrease of the reflectivity with the number of pulses related to the input fluence for (a) DCMS, (b) HiPIMS, and (c) RFMS. Note that for high fluences the data does not extend to 1000 pulses, as the detection camera automatically stopped upon catastrophic damage. (d) Energy ratio of the coating as a function of the input

fluence after 1000 shots for (green circle) HiPIMS, (blue square) DCMS, and (red triangle) RFMS. The dashed line represents the 1k-on-1 LIDT.

The energy ratio is defined as the reflected energy normalized to the first reflected pulse. The energy ratio on the aluminum coating made by DCMS (Figure 6a) doesn't show any decrease in reflectivity until the catastrophic damage is reached, with a reflectivity of more than 95% for every 1k-on-1 experiment (Figure 6d). Even after 1000 shots at 0.288 J/cm² (Figure 6d), almost no drop in reflectivity has been reported even though the 1k-on-1 LIDT is lower (i.e., 0.260 J/cm²). Discoloration has been observed after 1000 shots at a fluence between 0.260 and 0.288 J/cm² (Figure S5 and S6). Thus, the discoloration observed by Nomarski microscopy doesn't alter the reflective properties of this coating at the wavelength of the laser (1060 nm). The origin of the discoloration can be due to oxidation or contamination of the coating during LIDT. For aluminum coating made by HiPIMS (Figure 6b), the energy decrease can be seen even before the catastrophic damage is reached, with a drop of up to 20% of reflectivity after 1000 shots at 0.241 J/cm² (Figure 6d). To keep a decrease in reflectivity limited to 5% after 1000 shots, the input fluence should be limited to 0.232 J/cm². This value is lower than the 1k-on-1 LIDT reported earlier. A possible explanation for the discrepancy between DCMS and HiPIMS may lie in the differences in film microstructure, as the DCMS coating exhibits larger grains and, consequently, a lower density of grain boundaries (i.e., fewer defects). In the case of aluminum coating made by RFMS (Figure S7), the energy drop is more pronounced (Figure 6c). After 1000 shots at a fluence of 0.150 J/cm², a decrease of the reflectivity of 38% is observed (Figure 6d). When reaching the 1k-on-1 LIDT (i.e., 0.112 J/cm²), a reduction in the reflected fluence of the coating of more than 5% can be seen. The limited reflectivity properties from the RFMS-coated sample, even for low fluence, highlight the importance of having a smooth coating at the nanoscale to keep a reflectivity higher than 95% of the incoming beam with a high LIDT.

PLEASE CITE THIS ARTICLE AS DOI: 10.1063/5.0295260

This is the author's peer reviewed, accepted manuscript. However,

4 Conclusion

This study shows the influence of femtosecond laser beam irradiation at 1060 nm on an aluminum mirror coating. Aluminum coatings were made using three different magnetron sputtering discharges: DCMS, RFMS, and HiPIMS while keeping the same average power. The aluminum coating made by HiPIMS showed a similar structure to the DCMS one, exhibiting a 45-degree reflectance at 1060 nm and S-polarization of around 96%. Besides the similar 1k-on-1 LIDT (around 0.260 J/cm²), the DCMS coating reveals a decrease of the reflected power by 5% at higher fluence (0.288 J/cm²) than the aluminum coating made by HiPIMS (0.232 J/cm²). This study reveals the importance of investigating the fluence in the reflected beam to evaluate the LIDT of a highly reflective (HR) coating. We emphasize the importance of having a smooth coating at the nanoscale because the 1k-on-1 LIDT of the RFMS, which has a rough surface, drops significantly to 0.112 J/cm² compared to coatings from HIPIMS and DCMS. Additionally, grain boundaries appear detrimental to the F-LIDT performance, as shown by the lower threshold for the HiPIMS coating compared to the DCMS coating. Finally, the capability of using HiPIMS as a power source for magnetron sputtering for the synthesis of the optical coating is demonstrated. Despite a slight increase in the 1k-on-1 LIDT of the coating compared to DCMS. Further optimization of the HiPIMS process is expected to enhance the coating quality and increase the LIDT, paving the way toward high-performance coatings suitable for demanding applications such as ELI.

PLEASE CITE THIS ARTICLE AS DOI: 10.1063/5.0295260

This is the author's peer reviewed, accepted manuscript. However,

Supplementary material

The supplementary material provides (Figure S1) the characteristics of the laser beam used for the LIDT experiments. (Figure S2) A representative RGA spectrum of the LIDT chamber before experiments. (Figure S3) The surface topology map of aluminum coating. (Figure S4) The Rietveld refinement of the XRD patterns. (Figure S5) The 1k-on-1 LIDT data. (Figure S6 and S7) Differential Interference Contrast (DIC) images of the irradiated area after 1k-on-1 test.

Acknowledgements

Portions of this research were carried out at the ELI Beamlines Facility, a European user facility operated by the Extreme Light Infrastructure ERIC. This project has received funding from the European Union's HORIZON-INFRA-2022-TECH-01 call under grant agreement number 101095207. J. Zázvorka and M. Veis acknowledge funding from OPJAK – Ferroic multifunctionalities (FerrMion) CZ.02.01.01/00/22_008/0004591. S. Konstantinidis is Research Director of the National Fund for Scientific Research (FRS - FNRS Belgium).

References

¹ D. Ristau, editor, *Laser-Induced Damage in Optical Materials* (CRC Press, Boca Raton London New York, 2016).

² P. Poole, S. Trendafilov, G. Shvets, D. Smith, and E. Chowdhury, "Femtosecond laser damage threshold of pulse compression gratings for petawatt scale laser systems," Opt. Express **21**(22), 26341 (2013).

³ G.D. Tsibidis, "The influence of dynamical change of optical properties on the thermomechanical response and damage threshold of noble metals under femtosecond laser irradiation," J. Appl. Phys. **123**(8), 085903 (2018).

⁴ G.D. Tsibidis, D. Mansour, and E. Stratakis, "Damage threshold evaluation of thin metallic films exposed to femtosecond laser pulses: The role of material thickness," Opt. Laser Technol. **156**, 108484 (2022).

⁵ S.-S. Wellershoff, J. Hohlfeld, J. Güdde, and E. Matthias, "The role of electron–phonon coupling in femtosecond laser damage of metals:," Appl. Phys. Mater. Sci. Process. **69**(S1), S99–S107 (1999).

⁶ L. Gallais, D.-B. Douti, M. Commandré, G. Batavičiūtė, E. Pupka, M. Ščiuka, L. Smalakys, V. Sirutkaitis, and A. Melninkaitis, "Wavelength dependence of femtosecond laser-induced damage threshold of optical materials," J. Appl. Phys. **117**(22), 223103 (2015).

⁷ L.K. Ang, Y.Y. Lau, R.M. Gilgenbach, and H.L. Spindler, "Analysis of laser absorption on a rough metal surface," Appl. Phys. Lett. **70**(6), 696–698 (1997).

the online version of record will be different from this version once it has been copyedited and typeset. is the author's peer reviewed, accepted manuscript. However,

PLEASE CITE THIS ARTICLE AS DOI: 10.1063/5.0295260

- ⁸ P. Hruška, J. More-Chevalier, M. Novotný, J. Čížek, O. Melikhova, L. Fekete, M. Poupon, J. Bulíř, L. Volfová, M. Butterling, M.O. Liedke, A. Wagner, and P. Fitl, "Effect of roughness and nanoporosity on optical properties of black and reflective Al films prepared by magnetron sputtering," J. Alloys Compd. 872, 159744 (2021).
 ⁹ X. Cheng, and Z. Wang, "Defect-related properties of optical coatings," Adv. Opt. Technol. 3(1), 65–90 (2014).
- ¹⁰ W. Du, M. Zhu, J. Shi, T. Liu, J. Sun, K. Yi, and J. Shao, "Effect of subsurface impurity defects on laser damage resistance of beam splitter coatings," High Power Laser Sci. Eng. **11**, e61 (2023).
- ¹¹ J.B. Oliver, P. Kupinski, A.L. Rigatti, A.W. Schmid, J.C. Lambropoulos, S. Papernov, A. Kozlov, C. Smith, and R.D. Hand, "Stress compensation in hafnia/silica optical coatings by inclusion of alumina layers," Opt. Express **20**(15), 16596 (2012).
- ¹² C.J. Stolz, and R.A. Negres, "Ten-year summary of the Boulder Damage Symposium annual thin film laser damage competition," Opt. Eng. **57**(12), 1 (2018).
- ¹³ J.T. Gudmundsson, N. Brenning, D. Lundin, and U. Helmersson, "High power impulse magnetron sputtering discharge," J. Vac. Sci. Technol. Vac. Surf. Films **30**(3), 030801 (2012).
- ¹⁴ K. Sarakinos, J. Alami, and S. Konstantinidis, "High power pulsed magnetron sputtering: A review on scientific and engineering state of the art," Surf. Coat. Technol. **204**(11), 1661–1684 (2010).
- ¹⁵ C. Christou, and Z.H. Barber, "Ionization of sputtered material in a planar magnetron discharge," J. Vac. Sci. Technol. Vac. Surf. Films **18**(6), 2897–2907 (2000).
- ¹⁶ Y. Lifshitz, S.R. Kasi, and J.W. Rabalais, "Subplantation model for film growth from hyperthermal species: Application to diamond," Phys. Rev. Lett. **62**(11), 1290–1293 (1989).
- ¹⁷ H. Oettel, and R. Wiedemann, "Residual stresses in PVD hard coatings," Surf. Coat. Technol. **76–77**, 265–273 (1995).
- ¹⁸ D. Lundin, T. Minea, and J.T. Gudmundsson, editors, *High Power Impulse Magnetron Sputtering: Fundamentals, Technologies, Challenges and Applications* (Elsevier, Amsterdam, Netherlands, 2020).
- ¹⁹ J. Alami, S. Bolz, and K. Sarakinos, "High power pulsed magnetron sputtering: Fundamentals and applications," J. Alloys Compd. **483**(1–2), 530–534 (2009).
- ²⁰ F. Cemin, G. Abadias, T. Minea, and D. Lundin, "Tuning high power impulse magnetron sputtering discharge and substrate bias conditions to reduce the intrinsic stress of TiN thin films," Thin Solid Films **688**, 137335 (2019).
- ²¹ M. Hála, R. Vernhes, O. Zabeida, J.-E. Klemberg-Sapieha, and L. Martinu, "Reactive HiPIMS deposition of SiO2/Ta2O5 optical interference filters," J. Appl. Phys. **116**(21), 213302 (2014).
- ²² P.G. Bleotu, R. Udrea, A. Dumitru, O. Uteza, M.-D. Mihai, D.G. Matei, D. Ursescu, S. Irimiciuc, and V. Craciun, "Exploring fs-laser irradiation damage subthreshold behavior of dielectric mirrors via electrical measurements," High Power Laser Sci. Eng. 12, e15 (2024).
- ²³ D.-B.L. Douti, M. Chrayteh, S. Aknoun, T. Doualle, C. Hecquet, S. Monneret, and L. Gallais, "Quantitative phase imaging applied to laser damage detection and analysis," Appl. Opt. **54**(28), 8375 (2015).
- ²⁴ M. Sozet, J. Neauport, E. Lavastre, N. Roquin, L. Gallais, and L. Lamaignère, "Assessment of mono-shot measurement as a fast and accurate determination of the laser-induced damage threshold in the sub-picosecond regime," Opt. Lett. **41**(4), 804 (2016).
- ²⁵ J.Y. Natoli, J. Capoulade, B. Bertussi, M. Commandre, and H. Piombini, "Need to define a functional LIDT in multiple irradiation cases: examples of silica and KDP at 1064 nm and 355 nm," edited by G.J. Exarhos, A.H. Guenther, K.L. Lewis, D. Ristau, M.J. Soileau, and C.J. Stolz, (Boulder, CO, 2005), p. 599109.
- ²⁶ T.A. Laurence, D.A. Alessi, E. Feigenbaum, R.A. Negres, S.R. Qiu, C.W. Siders, T.M. Spinka, and C.J. Stolz, "Mirrors for petawatt lasers: Design principles, limitations, and solutions," J. Appl. Phys. **128**(7), 071101 (2020).
 ²⁷ G. Van Harten, F. Snik, and C.U. Keller, "Polarization Properties of Real Aluminum Mirrors, I. Influence of the Aluminum Oxide Layer," Publ. Astron. Soc. Pac. **121**(878), 377–383 (2009).
- ²⁸ A. Žutautas, S. Tamulevičius, and T. Tamulevičius, "From design to realization of high diffraction efficiency Littrow configuration diffraction gratings based on multilayer dielectric mirrors patterned with electron beam lithography," Opt. Laser Technol. **169**, 110086 (2024).
- ²⁹ S. Hädrich, J. Rothhardt, S. Demmler, M. Tschernajew, A. Hoffmann, M. Krebs, A. Liem, O. De Vries, M. Plötner, S. Fabian, T. Schreiber, J. Limpert, and A. Tünnermann, "Scalability of components for kW-level average power few-cycle lasers," Appl. Opt. **55**(7), 1636 (2016).
- ³⁰ A. Wajid, "On the accuracy of the quartz-crystal microbalance (QCM) in thin-film depositions," Sens. Actuators Phys. **63**(1), 41–46 (1997).
- ³¹ M. Lindner, and M. Schmid, "Thickness Measurement Methods for Physical Vapor Deposited Aluminum Coatings in Packaging Applications: A Review," Coatings 7(1), 9 (2017).
- ³² P.K. Velpula, D. Kramer, and B. Rus, "Femtosecond Laser-Induced Damage Characterization of Multilayer Dielectric Coatings," Coatings **10**(6), 603 (2020).
- ³³ Lasers and laser-related equipment Test methods for laser-induced damage threshold," (2025).
- ³⁴ N. Meidinger, S. Bonerz, H.W. Braeuninger, R. Eckhardt, J. Englhauser, R. Hartmann, G. Hasinger, P. Holl, N. Krause, G. Lutz, E. Pfeffermann, R.H. Richter, H. Soltau, L. Strueder, and J.E. Truemper, "Frame store PN-

PLEASE CITE THIS ARTICLE AS DOI: 10.1063/5.0295260

This is the author's peer reviewed, accepted manuscript. However,

- CCD detector for the ROSITA mission," edited by J.E. Truemper and H.D. Tananbaum, (Waikoloa, Hawai'i, United States, 2003), p. 1040.

 35 M. Samuelsson, D. Lundin, J. Jensen, M.A. Raadu, J.T. Gudmundsson, and U. Helmersson, "On the film
- ³⁵ M. Samuelsson, D. Lundin, J. Jensen, M.A. Raadu, J.T. Gudmundsson, and U. Helmersson, "On the filr density using high power impulse magnetron sputtering," Surf. Coat. Technol. **205**(2), 591–596 (2010).
- ³⁶ A. Nyaiesh, and L. Holland, "The dependence of deposition rate on power input for dc and rf magnetron sputtering," Vacuum **31**(7), 315–317 (1981).
- ³⁷ S. Wilbrandt, O. Stenzel, A. Liaf, P. Munzert, S. Schwinde, S. Stempfhuber, N. Felde, M. Trost, T. Seifert, and S. Schröder, "Spectrophotometric Characterization of Thin Semi-Transparent Aluminum Films Prepared by Electron Beam Evaporation and Magnetron Sputtering," Coatings **12**(9), 1278 (2022).
- ³⁸ Z. Matěj, A. Kadlecová, M. Janeček, L. Matějová, M. Dopita, and R. Kužel, "Refining bimodal microstructure of materials with MSTRUCT," Powder Diffr. **29**(S2), S35–S41 (2014).
- ³⁹ T. Roychowdhury, D. Shah, V. Jain, D.I. Patel, B. Dodson, W. Skinner, J.N. Hilfiker, S.J. Smith, and M.R. Linford, "Multi-instrument characterization of HiPIMS and DC magnetron sputtered tungsten and copper films," Surf. Interface Anal. **52**(7), 433–441 (2020).
- ⁴⁰ K. Aryal, H. Khatri, R.W. Collins, and S. Marsillac, "*In Situ* and *Ex Situ* Studies of Molybdenum Thin Films Deposited by rf and dc Magnetron Sputtering as a Back Contact for CIGS Solar Cells," Int. J. Photoenergy **2012**, 1–7 (2012).
- ⁴¹ S. Konstantinidis, A. Hemberg, J.P. Dauchot, and M. Hecq, "Deposition of zinc oxide layers by high-power impulse magnetron sputtering," J. Vac. Sci. Technol. B Microelectron. Nanometer Struct. Process. Meas. Phenom. **25**(3), L19–L21 (2007).
- ⁴² G. Abadias, E. Chason, J. Keckes, M. Sebastiani, G.B. Thompson, E. Barthel, G.L. Doll, C.E. Murray, C.H. Stoessel, and L. Martinu, "Review Article: Stress in thin films and coatings: Current status, challenges, and prospects," J. Vac. Sci. Technol. Vac. Surf. Films **36**(2), 020801 (2018).
- ⁴³ R.P.B. Viloan, U. Helmersson, and D. Lundin, "Copper thin films deposited using different ion acceleration strategies in HiPIMS," Surf. Coat. Technol. **422**, 127487 (2021).
- ⁴⁴ C.A. Davis, "A simple model for the formation of compressive stress in thin films by ion bombardment," Thin Solid Films **226**(1), 30–34 (1993).
- ⁴⁵ M. Kateb, J.T. Gudmundsson, P. Brault, A. Manolescu, and S. Ingvarsson, "On the role of ion potential energy in low energy HiPIMS deposition: An atomistic simulation," Surf. Coat. Technol. **426**, 127726 (2021).
- ⁴⁶ T.A. Germer, "Angular dependence and polarization of out-of-plane optical scattering from particulate contamination, subsurface defects, and surface microroughness," Appl. Opt. **36**(33), 8798 (1997).
- ⁴⁷ S. Schröder, M. Trost, M. Garrick, A. Duparré, X. Cheng, J. Zhang, and Z. Wang, "Origins of light scattering from thin film coatings," Thin Solid Films **592**, 248–255 (2015).
- ⁴⁸ H.E. Bennett, M. Silver, and E.J. Ashley, "Infrared Reflectance of Aluminum Evaporated in Ultra-High Vacuum," J. Opt. Soc. Am. **53**(9), 1089 (1963).
- ⁴⁹ I.-M. Vladisavlevici, D. Vizman, and E. d'Humières, "Laser Driven Electron Acceleration from Near-Critical Density Targets towards the Generation of High Energy γ-Photons," Photonics **9**(12), 953 (2022).
- ⁵⁰ X. Zhao, and Y.C. Shin, "Femtosecond laser ablation of aluminum in vacuum and air at high laser intensity," Appl. Surf. Sci. **283**, 94–99 (2013).
- ⁵¹ E.G. Gamaly, A.V. Rode, B. Luther-Davies, and V.T. Tikhonchuk, "Ablation of solids by femtosecond lasers: Ablation mechanism and ablation thresholds for metals and dielectrics," Phys. Plasmas **9**(3), 949–957 (2002).